HHS Public Access

Author manuscript

Environ Toxicol Pharmacol. Author manuscript; available in PMC 2024 March 01.

Published in final edited form as:

Environ Toxicol Pharmacol. 2023 March ; 98: 104070. doi:10.1016/j.etap.2023.104070.

Inhibition of Soluble Epoxide Hydrolase Reduces Paraquat Neurotoxicity in Rodents

Jogen Atone[a], **Karen Wagner**[a], **Shinichiro Koike**[b], **Jun Yang**[a], **Sung Hee Hwang**[a], **Bruce D. Hammock**[*,a]

[a]Department of Entomology and Nematology, and UC Davis Comprehensive Cancer Center, University of California Davis, Davis, CA 95616

[b]Department of Nutrition, University of California Davis, Davis, CA 95616

Abstract

Given the paucity of research surrounding the effect of chronic paraquat on striatal neurotoxicity, there is a need for further investigation into the neurotoxic effects of paraquat in mouse striatum. Furthermore, while previous studies have shown that inhibiting soluble epoxide hydrolase mitigates MPTP-mediated endoplasmic reticulum stress in mouse striatum, its effect on paraquat toxicity is still unknown. Thus, this study attempts to observe changes in inflammatory and endoplasmic reticulum stress markers in mouse striatum following chronic paraquat administration to determine whether inhibiting soluble epoxide hydrolase mitigates paraquat-induced neurotoxicity and whether it can reduce TLR4-mediated inflammation in primary astrocytes and microglia. Our results show that while the pro-inflammatory effect of chronic paraquat is small, there is a significant induction of inflammatory and cellular stress markers, such as COX2 and CHOP, that can be mitigated through a prophylactic administration of a soluble epoxide hydrolase inhibitor.

Keywords

paraquat; soluble epoxide hydrolase; anti-inflammatory drugs; Parkinson’s disease

1. Introduction

Paraquat (1,1’-dimethyl-4,4’-bipyridinium; PQ) is a non-selective contact herbicide used to control weeds and grasses around vegetables, grain, soybeans, coffee, cotton, and sugarcane among other crops (Bromilow, 2004). Recently, there has been a notable rise in PQ use within the US in the past decade, despite restrictions on its use, according to an estimate by the U.S. Geological Survey, reaching over 15 million pounds annually by 2018 (USGS, 2021). PQ has low dermal toxicity; however, its use is associated with numerous deaths following suicide attempts and accidental ingestion (Seok et al., 2009; Srikrishna et al., 1992). In addition to being one of the most acutely toxic pesticides worldwide (Dawson

[*]Corresponding author. Tel.: +1-530-752-7519, bdhammock@ucdavis.edu.

Conflict of interest statement: BD Hammock is a founder and KM Wagner is an employee of EicOsis L.L.C., a startup company with an sEH inhibitor in human clinical trials.

et al., 2010), PQ use has long been hypothesized to increase the risk of development of Parkinson's disease (PD) (Dinis-Oliveira et al., 2006; Tangamornsuksan et al., 2019). This is especially the case when PQ is combined with pesticides like the fungicide maneb (Bastias-Candia et al., 2019; Mandel et al., 2012), which is often a preferred experimental model given the inconsistency of toxic effects caused by PQ when administered by itself (Breckenridge et al., 2013; Jackson-Lewis et al., 2012; Thiruchelvam et al., 2000).

PQ is thought to exert its toxic effects through redox cycling with various metabolic enzymes or oxygen molecules, generating reactive oxygen species (ROS), which in turn cause apoptosis, endoplasmic reticulum (ER) stress, and inflammatory responses that exacerbate tissue damage (See et al., 2022; Wu et al., 2005). Following a systemic injection in mice, PQ accumulates in vital organs including the lung, kidney, liver, and brain, with a long tissue half-life such that a significant accumulation can occur in the brain (Breckenridge et al., 2013; Campbell et al., 2021). In mice, the half-life of PQ in the brain was approximately 3 weeks (Breckenridge et al., 2013). Such an ability for PQ to accumulate in mammalian tissues underscores the concern for chronic PQ exposure including subsequent toxic effects on the human population as well as the need for a therapeutic agent that can minimize the impact of PQ exposure (Fig. 1). Given that inflammation and ER stress often follow exposure to environmental neurotoxicants and accompany neurodegenerative disorders such as PD (McGeer and McGeer, 2004; Yang et al., 2020; Yoshida, 2007), a therapeutic agent that can mitigate both effects of neurotoxicity may be ideal. The soluble epoxide hydrolase (sEH), which metabolizes epoxy-fatty acids (EpFA) into their corresponding diols (Morisseau et al., 2010), is an enzyme known to have a role in modulating inflammation and ER stress. Small molecule inhibitors of the sEH are known to shift ER stress from initiation of inflammation, pain, and cell senescence toward cellular homeostasis and resolution of inflammation and pain (Atone et al., 2020; Wagner et al., 2017). Thus, sEH inhibitors may be valuable tools to reduce PQ-induced ER stress and inflammation, given that their mechanism involves reductions of inflammation, ER stress, apoptosis, and ROS among others (Atone et al., 2020).

Past research has studied sEH inhibitors as potential therapeutic candidates in numerous animal models of neuropathology, including stroke, traumatic brain injury, and 1-methyl-4-phenyl-1,2,3,6-tetrahydropyridine (MPTP)-induced neurotoxicity (Hung et al., 2017; Qin et al., 2015; Ren et al., 2018; Simpkins et al., 2009). While the precise mechanism of action of the EpFA is still under investigation, sEH inhibitors are known to increase the concentrations of endogenous EpFA, including the epoxyeicosatrienoic acids (EETs) derived from arachidonic acid. Like other classes of EpFA, EETs have been demonstrated to have anti-inflammatory and anti-apoptotic effects in numerous animal and cellular models (Hung et al., 2017; Tu et al., 2018). Several studies have demonstrated a neuroprotective effect of sEH inhibitors against dopaminergic neurotoxicants MPTP and rotenone through mitigation of inflammation, ER stress, and tyrosine hydroxylase (TH) loss (Lakkappa et al., 2019; Ren et al., 2018).

Several studies indicate that PQ can induce inflammation and ER stress (Li et al., 2015a; See et al., 2022; Yang et al., 2020). In addition, PQ is known to induce inflammation and ER stress in several organs of mice, most notably in the heart and lungs (Lei et

al., 2017). Given the broad systemic distribution of PQ and its accumulation in a mouse midbrain (Breckenridge et al., 2013), we hypothesized that inflammatory and ER stress markers would be elevated in the striatum following a 3-week administration of PQ. Further, we hypothesized that soluble epoxide hydrolase inhibitor 1-trifluoromethoxyphenyl-3-(1-propionylpiperidin-4-yl) urea (TPPU) would mitigate these endpoints of PQ-induced neurotoxicity. Finally, it is known that PQ does not cause direct glial activation in mice but does induce neuroinflammation through neural damage, inducing a TLR4-mediated activation (Klintworth et al., 2009; Wu et al., 2005; Yang et al., 2022). Here, we have assessed the effect of the TPPU and EETs on primary astrocytes and microglia activated by a TLR4 ligand LPS. Since it was previously shown that TPPU can be effective against LPS-induced glial inflammation in mice (Ghosh et al., 2020), we tested our hypothesis on rat glial cells with EETs regioisomers to expand our understanding of the scope of its therapeutic potential.

2. Methods

2.1 Chemicals

PQ was purchased from ThermoFisher (purity: 98%; Cat. 227320050, Lot: A0397584). MPTP was purchased from MedChemExpress (purity: >98%; Cat. HY-100852). LPS from *Salmonella typhosa* was purchased from MilliporeSigma (potency: >500000 EU/mg; Cat. L2387, Lot:117M4057V). EETs were synthesized and purified, as recently reported by Singh et al. (Singh et al., 2021). Purity was assessed via thin layer chromatography and nuclear magnetic resonance (data not shown). An inhibitor of soluble epoxide hydrolase TPPU was synthesized according to a previously published synthetic procedure (Rose et al., 2010b). ^{1}H NMR and ^{13}C NMR spectra were recorded at 400 and 100 MHz, respectively. Elemental analysis and FT-IR were determined at Robertson Microlit laboratories, Ledgewood, NJ. Mass spectra were measured by LC-MS equipped with an Agilent 1260 and a Bruker timsTOF Pro using electrospray (−) ionization. Source parameters were −4.25 kV capillary voltage, nebulizer gas at 2 bar, dry gas flow at 10 L/min, and temperature at 200 °C. The mass spectrometer was calibrated against sodium formate before acquiring the data to provide an accurate mass. The mobile phases are water with 0.1% acetic acid (A) and acetonitrile with 0.1% acetic acid (B). The gradient was from 5% B and increased to 95% B in 15 min. The separation was run on a Phenomenex Kinetex, 2.1×50 mm 1.7 um C18 column. Purity calculation (>99%; Fig. S1–4) was based on a reversed-phase LC / MS with total ion monitoring and a reversed LC chromatogram with monitoring at 254 nm. Only a single peak was detected in each chromatogram. In addition, the product was a single UV dense spot and a single spot based on phosphomolybdic acid spray and heating on normal phase TLC in hexane:ethyl ether 10:1.

The following parameters were used: ^{1}H NMR (400 MHz, DMSO-d_6) δ 8.56 (s, 1H), 7.47 (dd, J = 9 and 2 Hz, 2H), 7.21 (d, J = 9 Hz, 2H), 6.23 (d, J = 8 Hz, 1H), 4.19 (d, J = 13 Hz, 1H), 3.76 (d, J = 15 Hz, 1H), 3.72–3.66 (m, 1H), 3.12 (ddd, J = 14, 11, and 3 Hz, 1H), 2.78 (ddd, J = 14, 11, and 3 Hz, 1H), 2.31 (q, J = 7 Hz, 2H), 1.87–1.76 (m, 2H), 1.35–1.17 (m, 2H), 0.98 (t, J = 7 Hz, 3H). ^{13}C NMR (100 MHz, DMSO-d_6) δ 171.04, 154.33, 142.02, 139.73, 121.58, 120.20 (q, J = 255 Hz), 118.64, 46.29, 43.47, 39.82, 32.53, 31.77, 25.53,

9.48. IR (neat) 3308.86, 1634.77, 1602.03, 1572.04, 1531.96, 1505.62, 1440.77, 1303.97, 1256.23, 1204.79, 1160.28, 1131.68, 1105.16, 1072.67, 1042.49, 1014.54, 978.86, 921.03, 856.81, 795.81, 755.92 cm^{-1}. HRMS (*m*/*z*): [M + H]- calcd for $C_{16}H_{19}F_3N_3O_3$, 358.1378; found, 358.1377. Anal. Calcd for $C_{16}H_{20}F_3N_3O_3$: C, 53.48; H, 5.61; N, 11.69. Found: C, 53.49; H, 5.38; N, 11.70.

2.2 Animal Treatment

In-life procedures and husbandry performed at the University of California, Davis adhered to the guidelines of the National Institutes of Health Guide for the Care and Use of Laboratory Animals and were performed following the protocols approved by the Animal Use and Care Committee (IACUC) of the University of California, Davis. Male C57BL/6J mice (8–10 weeks; 20–25 g) were obtained from The Jackson Laboratory and were acclimated in our vivarium under a 12 h light/dark cycle for one week prior to pre-treatment with the sEH inhibitor (TPPU; 12 mg/L in 1% PEG-400 drinking water) or vehicle (1% PEG-400 in drinking water) control. The dose of TPPU was calculated based on the observed volume of water consumption (5 ml/day; Fig. S2) to yield approximately 2 mg/kg/day. Tail vein blood was sampled to quantify the TPPU concentration via LC-MS/MS to verify sufficient systemic exposure at the conclusion of the experiment (Fig. S1). The mice were assessed throughout the experiment for weight and water consumption (Fig. S2).

Formulated drinking water and chow were provided ad libitum. One week after the initiation of the treated drinking water, the mice were injected with either PQ (10 mg/kg, *i.p.*) or vehicle (sterile phosphate-buffered saline; PBS; ThermoFisher). PQ solutions were dissolved in sterile PBS, stored at −80°C until use, and injected into mice twice weekly for 3 weeks for 6 total injections. This dosage regime has been previously used for inducing chronic PQ neurotoxicity, with pharmacokinetic data verifying a chronic accumulation of PQ in mouse midbrain (Gupta et al., 2010; Prasad et al., 2009). Five days after the final PQ injection, the mice were euthanized via cervical dislocation upon inhalation of isoflurane anesthetic. Striatum samples between +1 mm and bregma were obtained on ice, washed in PBS, and flash frozen in liquid nitrogen for Western blot and RT-qPCR analysis. Alternatively, striatum samples were fixed in a 4% paraformaldehyde (PFA) solution in Phosphate-based saline (PBS; Apex Bioresearch Products; Cat. 20–134) for 48 hours, after which the samples were paraffinized and sectioned for immunohistochemical (IHC) analyses. Samples were obtained immediately after euthanasia without perfusion and thus contained small amounts of blood. The MPTP group received five intraperitoneal injections of MPTP (30 mg/kg/day) dissolved in PBS once a day, while the control group received sterile PBS (100 μL/day; *i.p.*) for five days. Mice were euthanized with isoflurane and cervical dislocation 1 week following the final injection, and their striata were either flash frozen for RT-qPCR or fixed in 4% PFA solution in PBS for subsequent paraffin embedding and IHC analysis.

2.3 Primary glial cell isolation and cell culture

Primary glial cells (>90% astrocytes) were isolated from the cortex of postnatal day 1–2 (P1–2) Sprague-Dawley rats (Charles River Laboratories). P1–2 rat pups were decapitated, the cortex isolated, dura and meninges removed, tissues mechanically homogenized with a sterile razor and triturated with a sterile fire-polished Pasteur pipette, and the resulting cells

strained using a 40 μm cell strainer (Spectrum Chemical). These cells were plated onto a T75 plate coated with poly-L-lysine (MilliporeSigma; molecular weight 150,000–300,000) at a density of 6.0×10^5 cells per cm^2 and cultured in DMEM (Corning) with 10% fetal bovine serum (FBS; ThermoFisher) for 8 days. On DIV 9, glial cells were plated onto a poly-L-lysine coated 96 well plate at a density of 6.25×10^5 cells per cm^2 and cultured overnight for experimentation the next day. The mixture consists of astrocytes and microglia, with approximately 90% GFAP+ astrocytes and 10% IBA+ microglia when assessed via immunocytochemistry (data not shown).

2.4 RT-qPCR

To assess the efficacy of the sEH substrates on glial cell activation, 1 μM each of EETs (14,15-EET, 11,12-EET, 8,9-EET, or a 1:1:1 mixture ratio), all ±1 μM TPPU in 10% FBS DMEM with 0.1% sterile DMSO were applied to primary rat glial cells (DIV 10). 5,6-EET was not included due to its unique susceptibility to nonenzymatic and/or cyclooxygenase-mediated cyclization (Carroll et al., 1993) and nonenzymatic conversion to the corresponding diol (DHET) (Jiang et al., 2004). The solutions of EETs and EETs mixtures and TPPU were prepared by adding them into DMSO and diluting in DMEM to give a final concentration of 1 μM, a level previously shown to reduce LPS-induced nitrite release in primary glial cells (Ghosh et al., 2020), with less than 0.1% DMSO at the final concentration in media. LPS dissolved in DMEM was then added to each well, and the cells were incubated at 37 °C for 24 h at a final concentration of 300 ng/ml. RNA was extracted using a TRIzol reagent according to the manufacturer's protocol. Alternatively, frozen striata collected from mice were pulverized, and RNA was extracted similarly using a TRIzol reagent. The RNA concentration and 260/280 values were assessed using NanoDrop Lite Spectrophotometer (ThermoFisher, Waltham, MA). For each reaction, 6 μL RNA (100 ng) was mixed with 9 μL Luna Universal One-Step RT-qPCR Kit Master Mix (Cat. E3005L, New England Biolabs) containing 8 μM of primers. The fluorescence was detected using Mic qPCR Cycler (Bio Molecular Systems, El Cajon, CA). Gene expression was calculated using the Ct values obtained within the Mic qPCR Analysis software, which uses the LinRedPCR method developed by Ramakers et al. (Ramakers et al., 2003). PCR product specificity was evaluated by melting curve analysis, with each product showing a single peak (data not shown). Primer sequences for RT-qPCR are listed in Table 1.

2.5 Western Blot

Mechanically pulverized frozen striatum samples were homogenized in radioimmunoprecipitation assay (RIPA) buffer (Neta Scientific) containing 1:100 protease inhibitor cocktail (MilliporeSigma), centrifuged for 30 minutes at 12,000 g at 4°C, and protein concentrations were assessed using a BCA assay (ThermoFisher). SDS-PAGE was performed on 10% SDS tris-glycine gels using 20 μg protein per lane (BioRad). The membranes were blocked using EveryBlot Blocking Buffer (BioRad) for 5 minutes, followed by primary antibody incubation overnight at 4°C in EveryBlot at 1:1000 concentration using the following antibodies: mouse anti-NFκB (Cell Signaling Cat. 8242S, Lot: 16), rabbit anti-ATF4 (Cell Signaling Cat. 11815S, Lot: 4), rabbit anti-eIF2α (Cell Signaling Cat. 5324S, Lot: 6), mouse anti-CHOP (Cell Signaling Cat. 2895S, Lot: 13), mouse anti-4-HNE (R&D Systems Cat. MAB3249, Lot: WXN0521121), and mouse

anti-β-actin (MilliporeSigma Cat. A5316, Lot: D0615). Membranes were incubated in anti-mouse or anti-rabbit horse radish peroxidase (HRP)-conjugated secondary antibodies (Cell Signaling) at 1:5000 in 0.1% TBS-T for 1 hour at room temperature. Enhanced chemiluminescence was performed using ProSignal Pico detection reagent (Genesee Scientific).

2.6 Immunohistochemistry

Striatum sections obtained from mice were fixed in a 4% paraformaldehyde in PBS for 48 hours, followed by a 70% ethanol solution for a week prior to paraffinization. Paraffin sections (5 μM sections) were prepared by the Histology Core within the UC Davis Department of Pathology and Laboratory Medicine. Sections were dewaxed in xylene and rehydrated using an ethanol gradient of 100%, 95%, 70%, 50%, 30%, and 0% ethanol in distilled water. Antigenic determinants were retrieved by microwaving the sections on high for 15 minutes in a 10 mM Na citrate (pH 6.0) solution. Endogenous peroxidases were inactivated by immersing sections in a 1% H_2O_2 solution for 15 minutes. Sections were blocked with 5% goat serum in PBS for 1 hour and stained overnight at 4 °C with 1:4000 tyrosine hydroxylase (TH) antibody (Cell Signaling, Cat. 2792, Lot: 6) in PBS with 2% goat plasma. Sections were then incubated with anti-rabbit biotinylated secondary antibody (Cell Signaling, Cat. 14708, Lot: 2) for 1 hour at room temperature in PBS with 2% goat plasma, and a signal was amplified using VECTASTAIN Elite ABC-HRP Kit (Vector Laboratories). The tissue was visualized using 3,3’-diaminobenzidine (DAB Substrate Kit for Peroxidase, Vector Laboratories), and sections were mounted using Cytoseal 60 (ThermoFisher). Slides were imaged at 4x magnification and analyzed using ImageJ image analysis software (ver.1.52).

2.7 Blood and plasma extraction and LC/MS analysis

Blood samples (10 μL) were collected from mice tail veins of control and TPPU-treated mice in an Eppendorf tube containing EDTA to yield a final EDTA concentration of 2 mg/ml 1 day prior to behavioral testing and euthanasia. TPPU was extracted using liquid-liquid extraction with 200 μL ethyl acetate, dried using a speed vacuum concentrator, and reconstituted in a 50 μL of 100 nM CUDA methanol solution. LC-MS/MS was conducted according to previously published methods (Wan et al., 2019). The liquid chromatography system used for analysis was an Agilent 1200 SL liquid chromatography series (Agilent Corporation, Palo Alto, CA). Liquid chromatography was performed on a PursuitPlus C18 2.0×150 mm, 5μm column (Varian Inc. Palo Alto, CA). Mobile phase A was water containing 0.1% glacial acetic acid, and mobile phase B consisted of acetonitrile with 0.1% glacial acetic acid. Gradient elution was performed at a flow rate of 250 μL/min. Eluted samples were analyzed using a 4000 QTrap tandem mass spectrometer (Applied Biosystems Instrument Corporation, Foster City, CA) equipped with an electrospray source (Turbo V). The instrument was operated in positive MRM mode. Similarly, mouse plasma was collected from cardiac puncture and centrifuged in an Eppendorf tube containing EDTA to yield a final EDTA concentration of 2 mg/ml. EET and DHET were extracted and analyzed using a previously published method (Yang et al., 2009). The instruments used were 6500 QTRAP+ (Sciex, Redwood City, CA) with Agilent 1260 UPLC system.

2.8 Statistical Analysis

All statistical analysis was carried out in Prism 9 analysis and graphing software (GraphPad ver. 9.3.1, San Diego, CA). One-way ANOVA with Dunnett's multiple comparisons post hoc test was used if variables satisfied Gaussian distributions tested by Bartlett's test. If not, Kruskal-Wallis test with Dunnett's multiple comparisons test was used. Results that were $p < 0.05$ were considered significant.

3. Results

3.1 PQ-mediated changes in inflammation and ER stress

Mice were pre-treated with the TPPU in drinking water for 1 week, followed by a continuous TPPU treatment and PQ injections twice weekly for 3 weeks. TPPU treatment in drinking water resulted in peripheral blood concentration of TPPU above 1 μM, orders of magnitude above the IC_{50} of 6 nM and K_i of 600 pM, and an increased 14,15-EET to 14,15-DHET ratio in plasma compared to vehicle controls (Fig. S5). There were no significant differences in the amount of water consumed or the weight of mice in the PQ group (Fig. S6) for the duration of the study. Chronic PQ administration significantly increased COX2 mRNA in striatal tissues ($p<0.05$; one-way ANOVA with Dunnett's post-hoc test), which was not significantly reduced by TPPU (Fig. 2).

Western blots for inflammatory markers NF-κB and 4-HNE, in addition to three ER stress markers ATF4, eIF2α, and CHOP, showed that chronic PQ treatment significantly increased only the chronic ER stress marker CHOP in the striata ($p=0.019$; one-way ANOVA with Dunnett's post-hoc test), which was reduced by TPPU ($p=0.008$) (Fig. 3). PQ did not result in a striatal TH loss of a similar magnitude as MPTP treatment. However, MPTP did not result in a higher inflammatory mRNA expression compared to PQ 1 week after the final MPTP injection (Fig. S7). MPTP treatment has resulted in a significant reduction of ATF4 gene expression compared to vehicle control ($p=0.039$, one-way ANOVA with Dunnett's post-hoc test), while no significant change was observed in COX2 or in any other inflammatory marker expressions. The level of sEH was not altered by either TPPU or PQ treatment (Fig. S8).

3.2 Reduction of TLR4-mediated inflammatory response by TPPU and EETs

Primary rat astrocytes and microglia mixture were pre-treated with TPPU with or without EETs regioisomers for 1 hour followed by 24 hours of LPS treatment, after which GAPDH normalized mRNA expressions of inflammatory markers IL-1β, IL-6, COX2, NOS2, CXCL1, and CXCL10 were assessed. While each of the EET regioisomers showed equivocal efficacy, when co-administered with TPPU, each EET regioisomer similarly reduced LPS-induced inflammation in glial cells ($p<0.05$, one-way ANOVA with Dunnett's post-hoc test). Combined 1:1:1 EET regioisomer with TPPU treatment significantly reduced LPS-induced IL-1β, IL-6, COX2, CXCL1, and CXCL10 mRNA expression ($p<0.05$, one-way ANOVA with Dunnett's post-hoc test) (Fig. 4). TPPU was particularly effective at improving the anti-inflammatory effects of 14,15-EET, significantly impacting the effect of 14,15-EET on reducing IL-1β, COX2, CXCL1, and CXCL10 mRNA ($p<0.05$, one-way ANOVA with Dunnett's post-hoc test) (Fig. 4).

4. Discussion

Our results indicate that chronic PQ administration significantly increased COX2 mRNA expression in the striata of mice 5 days after the final PQ injection, which was not significantly reduced by the TPPU treatment. Given the resulting peripheral blood concentration and the brain distribution of TPPU (Ghosh et al., 2020; Ostermann et al., 2015), this lack of effect is likely not due to dosing, absorption, or distribution of TPPU due to its high potency as an inhibitor, high target occupancy, and slow off rate from the target enzyme (Rose et al., 2010a). There was a small but significant increase in the ER stress protein CHOP expression, which was significantly reduced by TPPU. While we observed an unexpected reduction of the mRNA expression of TNF-α due to PQ, a trend not observed in the TPPU-treated PQ-intoxicated animals, the effect was not statistically significant. Given the large biological variability, slight changes in IL-1β, IL-6 mRNA, TNF-α mRNA, and 4-HNE were statistically non-significant. In addition, we observed a substantial TH loss in the mice striata 1 week after the final MPTP injection, whereas chronic PQ treatment showed no evidence of a TH loss. The lack of effect of PQ on striatal TH level was also observed in several other studies despite evidence of PQ accumulation in the midbrain (Breckenridge et al., 2013; Smeyne et al., 2016), contrary to other studies that demonstrated dopaminergic neurotoxicity due to chronic PQ injections (Prasad et al., 2009; Qin et al., 2015). Our findings support the published data suggesting that PQ may not be as toxic to striatal neurons despite modest but significant induction of CHOP and COX2 expression. However, the induction of CHOP and COX2 may facilitate dopaminergic neural loss over a more extended period of PQ exposure or alternatively exposure to PQ in conjunction with other pesticides such as maneb. While TPPU did not significantly reduce the induction of pro-inflammatory COX2 mRNA, the effect of TPPU on CHOP expression suggests that TPPU could potentially reduce PQ-induced neuronal loss since CHOP is a vital player in ER stress-mediated neurodegeneration (Li et al., 2015b).

Furthermore, our study offers insight into the efficacy of EET regioisomers in mitigating TLR4-dependent glial activation, which underlies the neuroinflammatory response against many environmental neurotoxicants, including PQ, organophosphate pesticides, dioxins, and ionizing radiation (Lucas and Maes, 2013; Yang et al., 2022). More specifically, we observed the effect of TPPU on enhancing the anti-inflammatory effect of all EET regioisomers that may be degraded by intracellular sEH activity, particularly of the 14,15-EET, which is also consistent with previous findings (Morisseau et al., 2010; Yu et al., 2000). Moreover, our data validated the anti-inflammatory effect of TPPU against TLR4-induced inflammation, hypothesized to underlie PQ-induced inflammation. The *in vitro* efficacy of TPPU in this prophylactic study offers avenues to investigate the effects of sEH inhibitors against xenobiotic-induced neuroinflammation and toxicity. Increased efficacy of EETs due to stabilization by the sEH inhibitor TPPU is consistent with previous findings on the presence of sEH enzyme expression and activity in mice and rat microglia and astrocytes (Atone et al., 2020).

It is important to note that there are limitations to our current study. First, while we did not observe severe inflammation in the striatum, it is important to note that the lack of severe inflammation in the striatum does not indicate a lack of general toxicity of PQ in

mice. Further studies are required to obtain a more comprehensive understanding of PQ toxicity in other organs such as the lung and heart. This remains vital given the potential health consequence of PQ's wide use throughout the world. Second, while PQ has long been associated with PD etiology, many of the behavioral symptoms observed in an MPTP PD model including tremors, rigidity, or akinesia (Taylor et al., 2010), have not been observed in this study. Preclinical studies indicate that PQ could act synergistically with the pesticide maneb (Gupta et al., 2010; Thiruchelvam et al., 2000) or iron (Peng et al., 2007), among others to induce PD-like symptoms in mice. However, reports indicate that there are nearly twice as many PD patients exposed to PQ alone compared to exposure to both PQ and maneb (Costello et al., 2009; Wang et al., 2011), suggesting that while maneb co-exposure could increase the risk of developing PD, effects and treatment options for exposure to PQ as a single entity should continue to be investigated.

Third, it is worth noting that we have used relatively young mice in this study. While the use of young mice to assess the impact of PQ toxicity is common in the field (Breckenridge et al., 2013), older mice exhibit PQ-induced dopaminergic neurotoxicity more robustly than younger mice (Thiruchelvam et al., 2003). This suggests that aged mice may be more suitable candidates to assess the efficacy of sEH inhibition against PQ toxicity. Therefore, a more in-depth study using multiple age groups is required to fully elucidate the magnitude of inflammatory and ER stress responses due to PQ exposure. Finally, we did not include sEHKO mice in this study given that sEHKO has previously been tested against PQ toxicity in mice (Qin et al., 2015). While off-target effects have not been reported for TPPU, future studies may expand the scope of treatments to sEH inhibitors with different pharmacophores and sEHKO mice to confirm the results obtained in this study.

5. Conclusion

To our knowledge, no attempts have been made prior to this study to determine whether an sEH inhibitor can be used prophylactically against PQ neurotoxicity in mice. This study adds to the evidence that PQ can induce striatal inflammation and ER stress in mice. In addition, this study demonstrates that while sEH inhibitor TPPU mitigates CHOP protein expression, it does not mitigate the COX2 mRNA expression. Given that there is evidence of synergism between the anti-inflammatory effects of sEH inhibitors and COX2 inhibitors (Zhang et al., 2014), this study also provides a rationale to probe the use of COX2/sEH dual inhibitors against PQ toxicity. Finally, given the lack of knowledge surrounding the regioisomer-specific effects of EETs on the glial activation (Atone et al., 2020), our study gives an insight into the discrepancies in anti-inflammatory effects among the EET regioisomers, providing an interesting avenue for further examination of the effects of EET regioisomers against TLR4-dependent inflammation.

While PQ is often implicated as an environmental contributor to the PD etiology (Bastias-Candia et al., 2019; Dwyer et al., 2021), its chronic neurological impact remains unclear, especially in regards to correlates such as age, gender, sex, genetic predispositions, as well as in regards to its interactions with other pesticides (Gupta et al., 2010; Picillo et al., 2017). As the chronic effects of PQ on human and animal health remain elusive, further research

into the neurotoxic impact of chronic PQ exposure, along with possible means to prevent or treat PQ toxicity, seems critically important to human and environmental health.

Supplementary Material

Refer to Web version on PubMed Central for supplementary material.

Acknowledgments:

This work was partially supported by the National Institute of Environmental Health Sciences RIVER award (R35 ES030443) and Superfund Research Program award (P42 ES004699), as well as the National Institute of Health CounterACT award (US54 NS127758). In addition, we would like to acknowledge the laboratory of Dr. Heike Wulff for their continuous support and guidance. The content is solely the responsibility of the authors and does not necessarily represent the official views of the National Institutes of Health.

References

Atone J, Wagner K, Hashimoto K, Hammock BD, 2020. Cytochrome P450 derived epoxidized fatty acids as a therapeutic tool against neuroinflammatory diseases. Prostaglandins Other Lipid Mediat 147, 106385. [PubMed: 31698143]

Bastias-Candia S, Zolezzi JM, Inestrosa NC, 2019. Revisiting the Paraquat-Induced Sporadic Parkinson's Disease-Like Model. Mol Neurobiol 56, 1044–1055. [PubMed: 29862459]

Breckenridge CB, Sturgess NC, Butt M, Wolf JC, Zadory D, Beck M, Mathews JM, Tisdel MO, Minnema D, Travis KZ, Cook AR, Botham PA, Smith LL, 2013. Pharmacokinetic, neurochemical, stereological and neuropathological studies on the potential effects of paraquat in the substantia nigra pars compacta and striatum of male C57BL/6J mice. Neurotoxicology 37, 1–14. [PubMed: 23523781]

Bromilow RH, 2004. Paraquat and sustainable agriculture. Pest Manag Sci 60, 340–349. [PubMed: 15119596]

Campbell JL Jr., Travis KZ, Clewell HJ 3rd, Stevens AJ, Hinderliter PM, Andersen ME, Botham PA, Cook AR, Minnema DJ, Wolf DC, 2021. Integration of paraquat pharmacokinetic data across species using PBPK modelling. Toxicol Appl Pharmacol 417, 115462. [PubMed: 33631233]

Carroll MA, Balazy M, Margiotta P, Falck JR, McGiff JC, 1993. Renal vasodilator activity of 5,6-epoxyeicosatrienoic acid depends upon conversion by cyclooxygenase and release of prostaglandins. J Biol Chem 268, 12260–12266. [PubMed: 8509363]

Costello S, Cockburn M, Bronstein J, Zhang X, Ritz B, 2009. Parkinson's disease and residential exposure to maneb and paraquat from agricultural applications in the central valley of California. Am J Epidemiol 169, 919–926. [PubMed: 19270050]

Dawson AH, Eddleston M, Senarathna L, Mohamed F, Gawarammana I, Bowe SJ, Manuweera G, Buckley NA, 2010. Acute human lethal toxicity of agricultural pesticides: a prospective cohort study. PLoS Med 7, e1000357. [PubMed: 21048990]

Dinis-Oliveira RJ, Remiao F, Carmo H, Duarte JA, Navarro AS, Bastos ML, Carvalho F, 2006. Paraquat exposure as an etiological factor of Parkinson's disease. Neurotoxicology 27, 1110–1122. [PubMed: 16815551]

Dwyer Z, Rudyk C, Farmer K, Beauchamp S, Shail P, Derksen A, Fortin T, Ventura K, Torres C, Ayoub K, Hayley S, 2021. Characterizing the protracted neurobiological and neuroanatomical effects of paraquat in a murine model of Parkinson's disease. Neurobiol Aging 100, 11–21. [PubMed: 33450723]

Ghosh A, Comerota MM, Wan D, Chen F, Propson NE, Hwang SH, Hammock BD, Zheng H, 2020. An epoxide hydrolase inhibitor reduces neuroinflammation in a mouse model of Alzheimer's disease. Sci Transl Med 12.

Gupta SP, Patel S, Yadav S, Singh AK, Singh S, Singh MP, 2010. Involvement of nitric oxide in maneb- and paraquat-induced Parkinson's disease phenotype in mouse: is there any link with lipid peroxidation? Neurochem Res 35, 1206–1213. [PubMed: 20455021]

Hung TH, Shyue SK, Wu CH, Chen CC, Lin CC, Chang CF, Chen SF, 2017. Deletion or inhibition of soluble epoxide hydrolase protects against brain damage and reduces microglia-mediated neuroinflammation in traumatic brain injury. Oncotarget 8, 103236–103260. [PubMed: 29262558]

Jackson-Lewis V, Blesa J, Przedborski S, 2012. Animal models of Parkinson's disease. Parkinsonism Relat Disord 18 Suppl 1, S183–185. [PubMed: 22166429]

Jiang H, McGiff JC, Quilley J, Sacerdoti D, Reddy LM, Falck JR, Zhang F, Lerea KM, Wong PY, 2004. Identification of 5,6-trans-epoxyeicosatrienoic acid in the phospholipids of red blood cells. J Biol Chem 279, 36412–36418. [PubMed: 15213230]

Klintworth H, Garden G, Xia Z, 2009. Rotenone and paraquat do not directly activate microglia or induce inflammatory cytokine release. Neurosci Lett 462, 1–5. [PubMed: 19559752]

Lakkappa N, Krishnamurthy PT, M DP, Hammock BD, Hwang SH, 2019. Soluble epoxide hydrolase inhibitor, APAU, protects dopaminergic neurons against rotenone induced neurotoxicity: Implications for Parkinson's disease. Neurotoxicology 70, 135–145. [PubMed: 30472438]

Lei Y, Li X, Yuan F, Liu L, Zhang J, Yang Y, Zhao J, Han Y, Ren J, Fu X, 2017. Toll-like receptor 4 ablation rescues against paraquat-triggered myocardial dysfunction: Role of ER stress and apoptosis. Environ Toxicol 32, 656–668. [PubMed: 27442881]

Li HF, Zhao SX, Xing BP, Sun ML, 2015a. Ulinastatin suppresses endoplasmic reticulum stress and apoptosis in the hippocampus of rats with acute paraquat poisoning. Neural Regen Res 10, 467–472. [PubMed: 25878598]

Li Y, Guo Y, Tang J, Jiang J, Chen Z, 2015b. New insights into the roles of CHOP-induced apoptosis in ER stress. Acta Biochim Biophys Sin (Shanghai) 47, 146–147. [PubMed: 25634437]

Lucas K, Maes M, 2013. Role of the Toll Like receptor (TLR) radical cycle in chronic inflammation: possible treatments targeting the TLR4 pathway. Mol Neurobiol 48, 190–204. [PubMed: 23436141]

Mandel JS, Adami HO, Cole P, 2012. Paraquat and Parkinson's disease: an overview of the epidemiology and a review of two recent studies. Regul Toxicol Pharmacol 62, 385–392. [PubMed: 22024235]

McGeer PL, McGeer EG, 2004. Inflammation and neurodegeneration in Parkinson's disease. Parkinsonism Relat Disord 10 Suppl 1, S3–7. [PubMed: 15109580]

Morisseau C, Inceoglu B, Schmelzer K, Tsai HJ, Jinks SL, Hegedus CM, Hammock BD, 2010. Naturally occurring monoepoxides of eicosapentaenoic acid and docosahexaenoic acid are bioactive antihyperalgesic lipids. J Lipid Res 51, 3481–3490. [PubMed: 20664072]

Ostermann AI, Herbers J, Willenberg I, Chen R, Hwang SH, Greite R, Morisseau C, Gueler F, Hammock BD, Schebb NH, 2015. Oral treatment of rodents with soluble epoxide hydrolase inhibitor 1-(1-propanoylpiperidin-4-yl)-3-[4-(trifluoromethoxy)phenyl]urea (TPPU): Resulting drug levels and modulation of oxylipin pattern. Prostaglandins Other Lipid Mediat 121, 131–137. [PubMed: 26117215]

Peng J, Peng L, Stevenson FF, Doctrow SR, Andersen JK, 2007. Iron and paraquat as synergistic environmental risk factors in sporadic Parkinson's disease accelerate age-related neurodegeneration. J Neurosci 27, 6914–6922. [PubMed: 17596439]

Picillo M, Nicoletti A, Fetoni V, Garavaglia B, Barone P, Pellecchia MT, 2017. The relevance of gender in Parkinson's disease: a review. J Neurol 264, 1583–1607. [PubMed: 28054129]

Prasad K, Tarasewicz E, Mathew J, Strickland PA, Buckley B, Richardson JR, Richfield EK, 2009. Toxicokinetics and toxicodynamics of paraquat accumulation in mouse brain. Exp Neurol 215, 358–367. [PubMed: 19084006]

Qin X, Wu Q, Lin L, Sun A, Liu S, Li X, Cao X, Gao T, Luo P, Zhu X, 2015. Soluble epoxide hydrolase deficiency or inhibition attenuates MPTP-induced parkinsonism. Molecular neurobiology 52, 187–195. [PubMed: 25128026]

Ramakers C, Ruijter JM, Deprez RH, Moorman AF, 2003. Assumption-free analysis of quantitative real-time polymerase chain reaction (PCR) data. Neurosci Lett 339, 62–66. [PubMed: 12618301]

Ren Q, Ma M, Yang J, Nonaka R, Yamaguchi A, Ishikawa K. i., Kobayashi K, Murayama S, Hwang SH, Saiki S, 2018. Soluble epoxide hydrolase plays a key role in the pathogenesis of Parkinson's disease. Proceedings of the National Academy of Sciences 115, E5815–E5823.

Rose TE, Morisseau C, Liu JY, Inceoglu B, Jones PD, Sanborn JR, Hammock BD, 2010a. 1-Aryl-3-(1-acylpiperidin-4-yl)urea Inhibitors of Human and Murine Soluble Epoxide Hydrolase: Structure-Activity Relationships, Pharmacokinetics, and Reduction of Inflammatory Pain. Journal of Medicinal Chemistry 53, 7067–7075. [PubMed: 20812725]

Rose TE, Morisseau C, Liu JY, Inceoglu B, Jones PD, Sanborn JR, Hammock BD, 2010b. 1-Aryl-3-(1-acylpiperidin-4-yl)urea inhibitors of human and murine soluble epoxide hydrolase: structure-activity relationships, pharmacokinetics, and reduction of inflammatory pain. J Med Chem 53, 7067–7075. [PubMed: 20812725]

See WZC, Naidu R, Tang KS, 2022. Cellular and Molecular Events Leading to Paraquat-Induced Apoptosis: Mechanistic Insights into Parkinson's Disease Pathophysiology. Mol Neurobiol 59, 3353–3369. [PubMed: 35306641]

Seok SJ, Gil HW, Jeong DS, Yang JO, Lee EY, Hong SY, 2009. Paraquat intoxication in subjects who attempt suicide: why they chose paraquat. Korean J Intern Med 24, 247–251. [PubMed: 19721862]

Simpkins AN, Rudic RD, Schreihofer DA, Roy S, Manhiani M, Tsai HJ, Hammock BD, Imig JD, 2009. Soluble epoxide inhibition is protective against cerebral ischemia via vascular and neural protection. Am J Pathol 174, 2086–2095. [PubMed: 19435785]

Singh N, Vik A, Lybrand DB, Morisseau C, Hammock BD, 2021. New Alkoxy- Analogues of Epoxyeicosatrienoic Acids Attenuate Cisplatin Nephrotoxicity In Vitro via Reduction of Mitochondrial Dysfunction, Oxidative Stress, Mitogen-Activated Protein Kinase Signaling, and Caspase Activation. Chem Res Toxicol 34, 2579–2591. [PubMed: 34817988]

Smeyne RJ, Breckenridge CB, Beck M, Jiao Y, Butt MT, Wolf JC, Zadory D, Minnema DJ, Sturgess NC, Travis KZ, Cook AR, Smith LL, Botham PA, 2016. Assessment of the Effects of MPTP and Paraquat on Dopaminergic Neurons and Microglia in the Substantia Nigra Pars Compacta of C57BL/6 Mice. PLoS One 11, e0164094. [PubMed: 27788145]

Srikrishna V, Riviere JE, Monteiro-Riviere NA, 1992. Cutaneous toxicity and absorption of paraquat in porcine skin. Toxicol Appl Pharmacol 115, 89–97. [PubMed: 1631899]

Tangamornsuksan W, Lohitnavy O, Sruamsiri R, Chaiyakunapruk N, Norman Scholfield C, Reisfeld B, Lohitnavy M, 2019. Paraquat exposure and Parkinson's disease: A systematic review and meta-analysis. Arch Environ Occup Health 74, 225–238. [PubMed: 30474499]

Taylor TN, Greene JG, Miller GW, 2010. Behavioral phenotyping of mouse models of Parkinson's disease. Behav Brain Res 211, 1–10. [PubMed: 20211655]

Thiruchelvam M, Brockel BJ, Richfield EK, Baggs RB, Cory-Slechta DA, 2000. Potentiated and preferential effects of combined paraquat and maneb on nigrostriatal dopamine systems: environmental risk factors for Parkinson's disease? Brain Res 873, 225–234. [PubMed: 10930548]

Thiruchelvam M, McCormack A, Richfield EK, Baggs RB, Tank AW, Di Monte DA, Cory-Slechta DA, 2003. Age-related irreversible progressive nigrostriatal dopaminergic neurotoxicity in the paraquat and maneb model of the Parkinson's disease phenotype. Eur J Neurosci 18, 589–600. [PubMed: 12911755]

Tu R, Armstrong J, Lee KSS, Hammock BD, Sapirstein A, Koehler RC, 2018. Soluble epoxide hydrolase inhibition decreases reperfusion injury after focal cerebral ischemia. Sci Rep 8, 5279. [PubMed: 29588470]

USGS, 2021. Estimated Annual Agricultural Pesticide Use, Pesticide National Synthesis Project, https://water.usgs.gov/nawqa/pnsp/usage/maps/show_map.php?year=2018&map=PARAQUAT&hilo=H.

Wagner KM, McReynolds CB, Schmidt WK, Hammock BD, 2017. Soluble epoxide hydrolase as a therapeutic target for pain, inflammatory and neurodegenerative diseases. Pharmacol Ther 180, 62–76. [PubMed: 28642117]

Wan D, Yang J, McReynolds CB, Barnych B, Wagner KM, Morisseau C, Hwang SH, Sun J, Blocher R, Hammock BD, 2019. In vitro and in vivo Metabolism of a Potent Inhibitor of Soluble Epoxide Hydrolase, 1-(1-Propionylpiperidin-4-yl)-3-(4-(trifluoromethoxy)phenyl)urea. Front Pharmacol 10, 464. [PubMed: 31143115]

Wang A, Costello S, Cockburn M, Zhang X, Bronstein J, Ritz B, 2011. Parkinson's disease risk from ambient exposure to pesticides. Eur J Epidemiol 26, 547–555. [PubMed: 21505849]

Wu XF, Block ML, Zhang W, Qin L, Wilson B, Zhang WQ, Veronesi B, Hong JS, 2005. The role of microglia in paraquat-induced dopaminergic neurotoxicity. Antioxid Redox Signal 7, 654–661. [PubMed: 15890010]

Yang HM, Wang YL, Liu CY, Zhou YT, Zhang XF, 2022. A time-course study of microglial activation and dopaminergic neuron loss in the substantia nigra of mice with paraquat-induced Parkinson's disease. Food Chem Toxicol 164, 113018. [PubMed: 35430334]

Yang J, Schmelzer K, Georgi K, Hammock BD, 2009. Quantitative profiling method for oxylipin metabolome by liquid chromatography electrospray ionization tandem mass spectrometry. Anal Chem 81, 8085–8093. [PubMed: 19715299]

Yang Z, Shao Y, Zhao Y, Li Q, Li R, Xiao H, Zhang F, Zhang Y, Chang X, Zhang Y, Zhou Z, 2020. Endoplasmic reticulum stress-related neuroinflammation and neural stem cells decrease in mice exposure to paraquat. Sci Rep 10, 17757. [PubMed: 33082501]

Yoshida H, 2007. ER stress and diseases. FEBS J 274, 630–658. [PubMed: 17288551]

Yu Z, Xu F, Huse LM, Morisseau C, Draper AJ, Newman JW, Parker C, Graham L, Engler MM, Hammock BD, Zeldin DC, Kroetz DL, 2000. Soluble epoxide hydrolase regulates hydrolysis of vasoactive epoxyeicosatrienoic acids. Circ Res 87, 992–998. [PubMed: 11090543]

Zhang G, Panigrahy D, Hwang SH, Yang J, Mahakian LM, Wettersten HI, Liu JY, Wang Y, Ingham ES, Tam S, Kieran MW, Weiss RH, Ferrara KW, Hammock BD, 2014. Dual inhibition of cyclooxygenase-2 and soluble epoxide hydrolase synergistically suppresses primary tumor growth and metastasis. Proc Natl Acad Sci U S A 111, 11127–11132. [PubMed: 25024195]

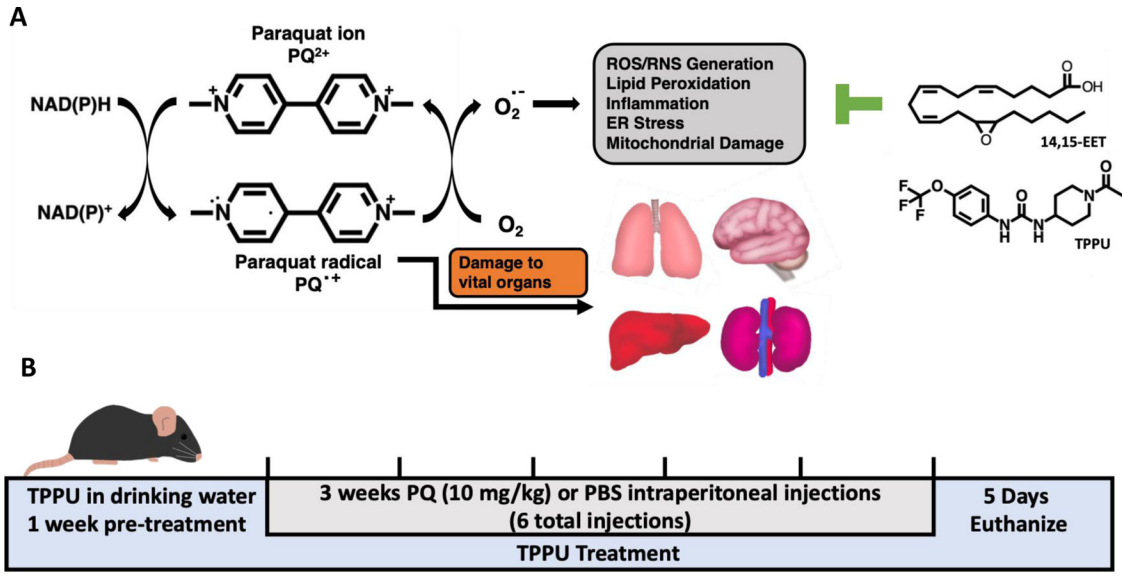

Figure 1.

Schematic representations of the **A.** mechanism of PQ toxicity showing the structure of PQ and its radical form, as well as the 14,15-EET regioisomer and sEH inhibitor TPPU which stabilizes EpFA from hydrolysis by the sEH, and **B.** timeline of PQ injections in mice. PQ is thought to exert its toxic effects through redox cycling, whereby a PQ ion is converted into a PQ radical through a transfer of electrons from donors such as cytosolic NAD(P)H, which then generates oxygen radical leading to oxidative damage, lipid peroxidation, inflammation, ER stress, mitochondrial damage, and apoptosis. Acute exposure to PQ could result in kidney, liver, or respiratory failure, whereas long-term exposure to PQ may result in pulmonary fibrosis or damage to kidneys and heart. In addition, several studies have shown that PQ also distributes to and accumulates in the brain. Inhibitors of sEH enzyme acting to stabilize EpFA, such as EETs, are known to reduce inflammation, ER stress, pathological fibrosis, and apoptosis in many animal models. Therefore, we hypothesize that the administration of the sEH inhibitor TPPU will mitigate inflammation and ER stress in the brains of mice exposed to PQ.

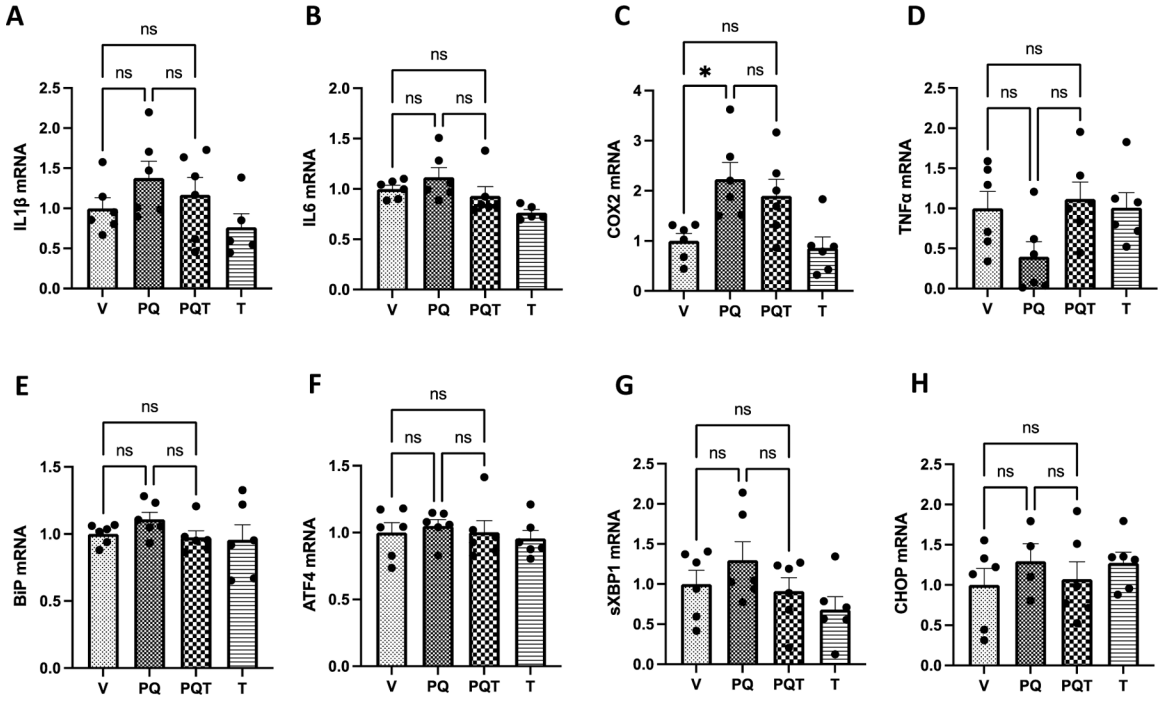

Figure 2.

Effect of PQ and TPPU on striatal GAPDH normalized mRNA expressions of pro-inflammatory (**A-D**) and ER stress (**E-H**) markers. Chronic PQ treatment caused a non-significant increase of inflammatory genes **A.** IL-1β and **B.** IL-6 and a significant change in **C.** COX2 expression (p=0.0122). **D.** While there was some reduction of TNF-α in the PQ group (p=0.131) that was reversed by TPPU treatment (p=0.056), such effects were not statistically significant. However, the reduction of IL-1β, IL-6, and COX2 expressions by TPPU was not statistically significant. There was no detectable trend in changes in any of the ER stress gene expressions (**E-H**). Results are expressed as mean ± SEM. RT-qPCR, data represent 5 or 6 biological replicates. PCR results were normalized to respective GAPDH levels. Abbreviations: V = vehicle, PQ = paraquat, PQT = paraquat, TPPU, T = TPPU only control. *P < 0.05 and **P<0.01, as determined by one-way ANOVA or Kruskal-Wallis test followed by Dunnett's post-hoc test.

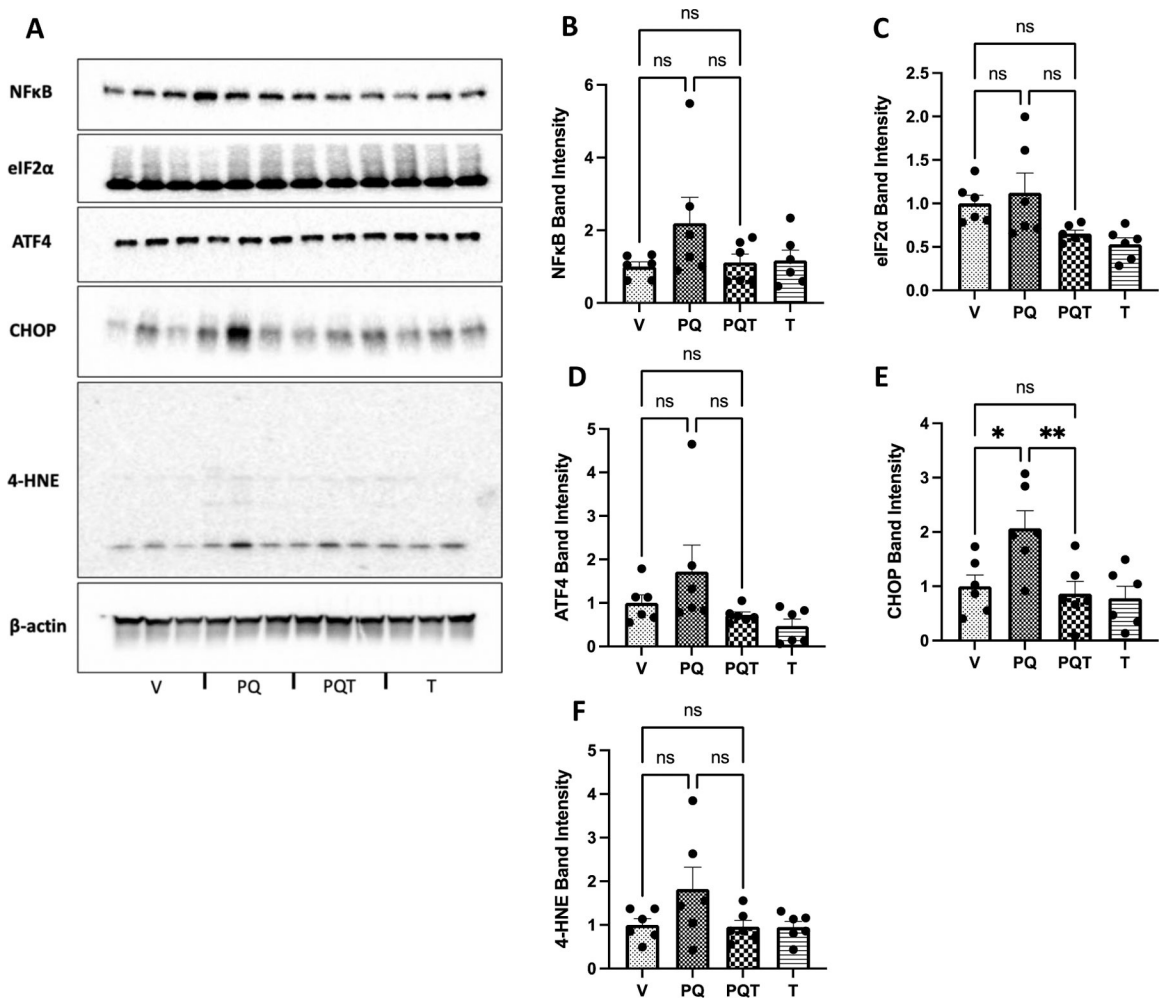

Figure 3.

A. Western blot analysis of frozen striatum samples assessing protein levels of **B.** NF-κB, **C.** ATF4, **D.** eIF2α, **E.** CHOP, and **H.** 4-HNE. While PQ significantly increased CHOP protein expression (p=0.019), which was reduced by TPPU treatment (p=0.008), increases in other proteins due to PQ treatment were not statistically significant. Results are expressed as mean ± SEM; data represent 6 biological replicates. Western Blot results were normalized to β-actin. Abbreviations: V = vehicle, PQ = paraquat, PQT = paraquat and TPPU, T = TPPU only control. Results are expressed as mean ± SEM. *P < 0.05 and **P<0.01, as determined by one-way ANOVA or Kruskal-Wallis test followed by Dunnett's post-hoc test.

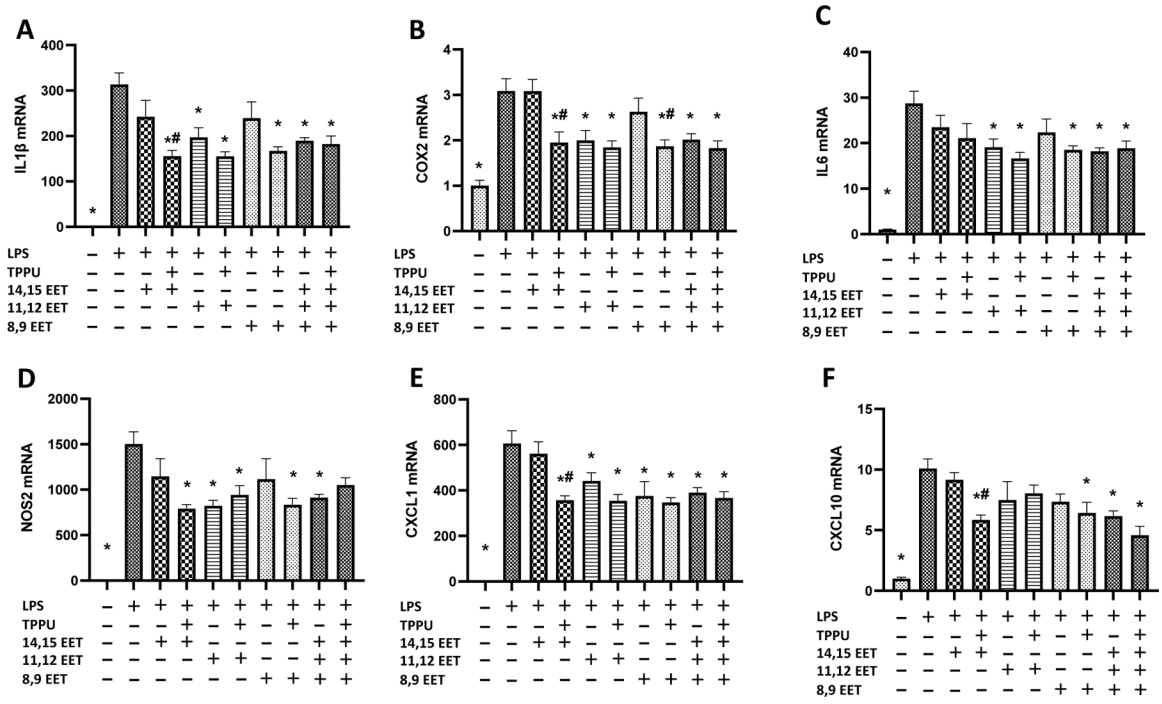

Figure 4.

Primary rat glial cells (DIV 8–10) were pretreated with 1 μM of EET regioisomers in the absence or presence of TPPU (1 μM) and were then incubated with 300 ng/ml LPS in 100 μL DMEM for 24 hours. (**A-F**) LPS significantly increased inflammatory markers IL-1β, IL-6, COX2, NOS2, CXCL1, and CXCL10 mRNA expression (n=5 or 6 technical replicates, $p<0.001$), which were mitigated by EETs regioisomers, with a 1:1:1 ratio mixture of three EETs regioisomers, or EETs with TPPU cotreatment. While EETs regioisomers showed equivocal efficacy against LPS-induced inflammation, most EETs regioisomers mitigated LPS-induced inflammation when co-treated with TPPU ($p<0.05$). More specifically, TPPU treatment resulted in a significant reduction of IL-1β, COX2, CXCL1, and CXCL10 expressions when combined with 14,15-EET, and COX2 expression when combined with 8,9-EET ($p<0.05$). Results are expressed as mean ± SEM. Statistical significance was determined by one-way ANOVA followed by Dunnett's post-hoc test (* $p<0.05$ compared to LPS; # $p<0.05$ compared to respective EET regioisomer without TPPU).

Table 1.

Primer sequences for mouse and rat genes analyzed with RT-qPCR

Gene	Type	Sequence (5'−3')
Mouse primers for brain tissue		
ATF4	Forward	GACCTGGAAACCATGCCAGA
	Reverse	TGGCCAATTGGGTTCACTGT
BiP	Forward	ACTTGGGGACCACCTATTCCT
	Reverse	ATCGCCAATCAGACGCTCC
CHOP	Forward	CCCTGCCTTTCACCTTGG
	Reverse	CCGCTCGTTCTCCTGCTC
COX2	Forward	CAGACAACATAAACTGCGCCTT
	Reverse	GATACACCTCTCCACCAATGACC
GAPDH	Forward	CGTGTTCCTACCCCCAATGT
	Reverse	GTGTAGCCCAAGATGCCCTT
IL-1β	Forward	CCTTCCAGGATGAGGACATGA
	Reverse	TGAGTCACAGAGGATGGGCTC
sXBP1	Forward	GGTCTGCTGAGTCCGCAGCAGG
	Reverse	AGGCTTGGTGTATACATGG
TNF-α	Forward	GCCACCACGCTCTTCTGT
	Reverse	GGAGGCCATTTGGGAACT
Rat primers for cell culture		
CXCL1	Forward	ACTCAAGAATGGTCGCGAGG
	Reverse	ACGCCATCGGTGCAATCTAT
CXCL10	Forward	CGGTGAGCCAAAGAAGGTCTA
	Reverse	TGTCCATCGGTCTCAGCACT
GAPDH	Forward	CCAGGGCTGCCTTCTCTTGT
	Reverse	GTTTCCCGTTGATGACCAGC
GDNF	Forward	CACCAGATAAACAAGCGGCG
	Reverse	TCGTAGCCCAAACCCAAGTC
IL-1β	Forward	CTACCTATGTCTTGCCCGTGG
	Reverse	CACACTAGCAGGTCGTCATCA
IL-6	Forward	GGCTAAGGACCAAGACCATCC
	Reverse	GACCACAGTGAGGAATGTCCA
NOS2	Forward	TTTGACCAGAGGACCCAGAGA
	Reverse	CAGAGTGAGCTGGTAGGTTCC
COX2	Forward	ACGGTGAAACTCTAGACAGACA
	Reverse	AGGATACACCTCTCCACCGA